Title

Two-photon microperimetry with picosecond pulses.

Journal

Biomedical Optics Express, 12(1)

ISSN

2156-7085

Authors

Marzejon, Marcin
Kornaszewski, Łukasz
Bogusławski, Jakub
et al.

Publication Date

2021

DOI

10.1364/BOE.411168

Peer reviewed

Research Article | Vol. 12, No. 1 / 1 January 2021 / Biomedical Optics Express 462
Biomedical Optics EXPRESS

Two-photon microperimetry with picosecond pulses

MARCIN J. MARZEJON,[1,2,3] ŁUKASZ KORNASZEWSKI,[1,3] JAKUB BOGUSŁAWSKI,[1,3] PIOTR CIĄĆKA,[1,3] MIŁOSZ MARTYNOW,[4,5] GRAŻYNA PALCZEWSKA,[3,6,7] SEBASTIAN MAĆKOWSKI,[4,8] KRZYSZTOF PALCZEWSKI,[3,7,9,10] MACIEJ WOJTKOWSKI,[1,3,4,8] AND KATARZYNA KOMAR[3,4,8,*]

[1]*Institute of Physical Chemistry, Polish Academy of Sciences, Kasprzaka 44/52, 01-224 Warszawa, Poland*
[2]*Department of Metrology and Optoelectronics, Faculty of Electronics, Telecommunications and Informatics, Gdańsk University of Technology, G. Narutowicza 11/12, 80-223 Gdańsk, Poland*
[3]*International Centre for Translational Eye Research, Institute of Physical Chemistry, PAS, Skierniewicka 10a, 01-230 Warszawa, Poland*
[4]*Baltic Institute of Technology, Al. Zwycięstwa 96/98, 81-451 Gdynia, Poland*
[5]*Department of Theoretical Physics and Quantum Information, Faculty of Applied Physics and Mathematics, Gdańsk University of Technology, G. Narutowicza 11/12, 80-233 Gdańsk, Poland*
[6]*Polgenix, Inc., Department of Medical Devices, Cleveland OH 44106, USA*
[7]*Gavin Herbert Eye Institute, Department of Ophthalmology, University of California, Irvine, CA 92697, USA*
[8]*Institute of Physics, Faculty of Physics, Astronomy and Informatics, Nicolaus Copernicus University in Torun, Grudziądzka 5, 87-100 Toruń, Poland*
[9]*Department of Physiology & Biophysics, School of Medicine, University of California, Irvine, CA 926978, USA*
[10]*Department of Chemistry, University of California, Irvine, CA 926978, USA*
[*]*kkomar@fizyka.umk.pl*

Abstract: Two-photon vision is a phenomenon associated with the perception of short pulses of near-infrared radiation (900-1200 nm) as a visible light. It is caused by the nonlinear process of two-photon absorption by visual pigments. Here we present results showing the influence of pulse duration and repetition rate of short pulsed lasers on the visual threshold. We compared two-photon sensitivity maps of the retina obtained for subjects with normal vision using a cost-effective fiber laser ($\lambda_c = 1028.4$ nm, $\tau_p = 12.2$ ps, $F_{rep} = 19.17$ MHz) and a solid-state laser ($\lambda_c = 1043.3$ nm, $\tau_p = 0.253$ ps, $F_{rep} = 62.65$ MHz). We have shown that in accordance with the description of two-photon absorption, the average optical power required for two-photon vision for a fiber laser is 4 times greater than that for a solid-state laser. Mean sensitivity measured for the first one is 5.9 ± 2.8 dB lower than for the second but still 17 dB away from the safety limit, confirming that picosecond light sources can be successfully applied in microperimetry. This development would dramatically reduce the cost and complexity of future clinical devices.

1. Introduction

Perimetry, a method of testing patient's visual field by determining the thresholds of vision, plays an important role in ophthalmological diagnostics, because it provides direct information about the functional properties of the retina. Quantifying function is essential for monitoring disease progression and the efficacy of treatments and, importantly, functional impairment often precedes the structural changes detected by most imaging modalities. Perimetry is most notable for assessing the progression of glaucoma [1]. Still, there are other ocular diseases for which mapping the sensitivity of the retina to light is important during treatment like neovascular and

#411168 https://doi.org/10.1364/BOE.411168
Journal © 2021 Received 29 Sep 2020; revised 23 Nov 2020; accepted 24 Nov 2020; published 17 Dec 2020

Biomedical Optics EXPRESS

degenerative events associated with diabetic retinopathy [2], age-related macular degeneration [3], and Stargardt disease [4]. Mapping visual function is also useful for the diagnosis of neurological disorders and traumatic injuries to the brain [5].

The development of visual field mapping began with manual methods employing a tangent screen in a classic Goldmann perimeter, and now extends to automated perimeters and microperimeters [6,7]. Automated perimetry applies more efficient strategies for determining the visibility threshold, sometimes optimized for detecting the profile of a particular disease [8]. The combination of perimetry with SLO (scanning laser ophthalmoscopy), OCT (optical coherence tomography), or fundus camera imaging allows for precise stimulation of specific retinal regions to correlate structural alterations with functional impairment [9]. The accuracy of stimulation has been further improved in laboratory systems, using adaptive optics imaging and advanced retinal tracking, at the resolution of a single cell [10,11]. All the techniques mentioned above examine the sensitivity of the retina to visible light, spanning wavelengths between 400-720 nm. In this study we have tested retinal sensitivity to pulsed near-infrared (IR) light (~1000 nm) based on *two-photon vision* [12–15], which was incorporated into visual field testing as *two-photon microperimetry* [14].

The phenomenon called *two-photon vision* was described originally for 200 femtosecond laser pulses, enlongated by dispersion in the optical fiber to ~1 ps [12]. Shifting the stimulus wavelength resulted in the change of the perceived color from blue (~475 nm) for 950 nm IR light to red (~600 nm) for 1200 nm IR light [12]. Furthermore, starting from 900 nm, the sensitivities of dark adapted human observers [15], as well as the magnitude of ERG responses of murine and primate photoreceptors [12,16], did not decrease as the wavelength increased up to 1000 nm. These observations violated the well-established relationship (for one-photon vision) of a linear decline in the logarithm of sensitivity versus wavelength [17,18]. With humans at 1000 nm IR light, sensitivity was 1.5-2 orders of magnitude higher than expected for one-photon vision at this wavelength [12]. Molecular modeling employing hybrid quantum-mechanical calculations coupled with molecular dynamics simulations confirmed the feasibility of two-photon isomerization of rhodopsin by IR light with a maximum absorption around 1000 nm [12,19]. Further investigations demonstrated that the relationship between 522.5 nm and 1045 nm visibility thresholds was almost quadratic when using femtosecond pulses, thus confirming the nonlinear character of IR light perception [14]. Manzanera et al. supported these observations by testing an extreme case of using a supercontinuum light source with nanosecond pulses and repetition rates of single kHz [20]. However, using pulsed sources of such extremely low repetition rates causes the visual threshold and MPE level to become close to each other, so that practical application of such sources in the clinical setting is questionable due to safety issues. Interestingly, weak two-photon vision effects were also observed in OCTs using short cavity swept-sources due to their multimode operation and the presence of a mode-locking process enabling generation of nanosecond impulses [21,22].

Perception of light based on two-photon excitation depends on the square of stimulus intensity; while normal, one-photon perception depends on intensity linearly. There are two main differences between these two kinds of light perception: (1) perception of stimuli changes more rapidly with increase/decrease of power for two-photon vision compared to one-photon vision; (2) infrared light, used in two-photon perimetry, is impacted less by imperfections in the front of the eye than visible light, as shown by [14]. The first difference suggests that determination of visual threshold on the basis of two-photon perception would be more precise: a 2-times less intense beam would result in a 4-times dimmer stimulus. Consequently, transition from seen to unseen stimulus would cover a smaller range of intensities. This feature can be also demonstrated by comparison of the shapes of psychometric functions for these two ways of vision: the slope of psychometric function for two-photon vision is steeper than for normal vision [14]. The second difference, however could have negative impact because small changes in stimulus size caused by optical

Biomedical Optics EXPRESS

imperfections in different eyes may be more detrimental for visibility thresholds with two-photon perceived stimuli than with the ones derived from one-photon vision. The question if two-photon based perimetry is better than one-photon perimetry depends on which difference prevails in visual threshold testing. Further investigations are definitely required, involving participation of different groups of ophthalmic patients. Therefore, it is essential to characterize and develop the technique to make it more clinically applicable.

The medical applicability of two-photon microperimetry depends largely on the parameters of the laser used for experiments. The safety standards defining Maximum Permissible Exposure (MPE) are an absolute limitation. The lowest perceived value of the power corresponding to the visual threshold depends on pulse duration and repetition rate. The optimal method from the point of view of the applicability of the method is to choose the parameters which will guarantee the largest range of powers spanning between the visual threshold and the MPE. This can be achieved with the use of femtosecond solid-state lasers, which are expensive and hard to adapt to the clinics. Another extreme case is to use a light source emitting in a longer, nanosecond regime like the supercontinuum [20,23]. In such a case, the optical power values corresponding to the two-photon visual thresholds are only 10 times lower than the values corresponding to the Maximum Permissible Exposure limit [20]. Such a narrow range of stimulus intensities does not guarantee the emergence of the two-photon vision effect in all examined patients. Fiber lasers emitting picosecond pulses extend that range. Furthermore, these lasers are several times less expensive and much easier to integrate into diagnostic devices because of their smaller size, less demanding cooling requirements, and fiber output, which is easy to integrate with the system's optics. These features, in turn, support the transfer of the technique from specialized optical laboratories to clinics, ophthalmological surgeries, etc.

In this report, we present analyses leading to the optimization of two-photon microperimeter by selecting pulse durations and laser repetition rates. We compare two-photon sensitivity maps of the parafoveal region of dark adapted subjects obtained using the same two-photon microperimeter operating with two different pulsing near-infrared lasers: a femtosecond solid-state laser, referred to as "*fs laser*", and a compact picosecond fiber laser, designed for our experiment and referred to as "*ps laser*". Moreover, we propose a model which takes into account how differences in the temporal aspects of the pulse train and individual pulses impact the two-photon visibility threshold. Finally, we discuss how spectral and geometric differences between both laser beams influenced the threshold.

2. Methods

2.1. Optical setup of the laboratory two-photon perimeter

The optical scheme of the laboratory perimeter for mapping two-photon sensitivity for both lasers is presented in Fig. 1.

Fs laser beam was guided into the apparatus using two deflecting mirrors (M_1, M_2 in Fig. 1) after passing through a reflective gradient neutral density filter GF_1 to reduce its power. The telescope consisting of lenses L_1 and L_2 was used only during a subset of measurements (described in detail in Section 4), to exactly match the diameters of both beams at the eye's pupil plane. *Ps laser* beam was collimated at the fiber output by a 19 mm lens, CL and introduced into the system using mirror M_3 and a beamsplitter BS_1. An additional neutral density filter (F in Fig. 1) was used to reduce the laser beam power. Then, beams were routed through an additional polarizing beamsplitter, polBS (inserted for introducing a visible laser, although one was not used in this study) and aperture A, which was optically conjugated with galvanometric scanners, GSC (GVS002, Thorlabs) by the telescope consisting of lenses L_3 and L_4 of the same focal length, equal to 150 mm.

The intensity of the stimulating light during measurements was adjusted using a round reflective variable neutral density filter GF_2 (NDC-50C-4, Thorlabs). The optical density of this filter

Biomedical Optics EXPRESS

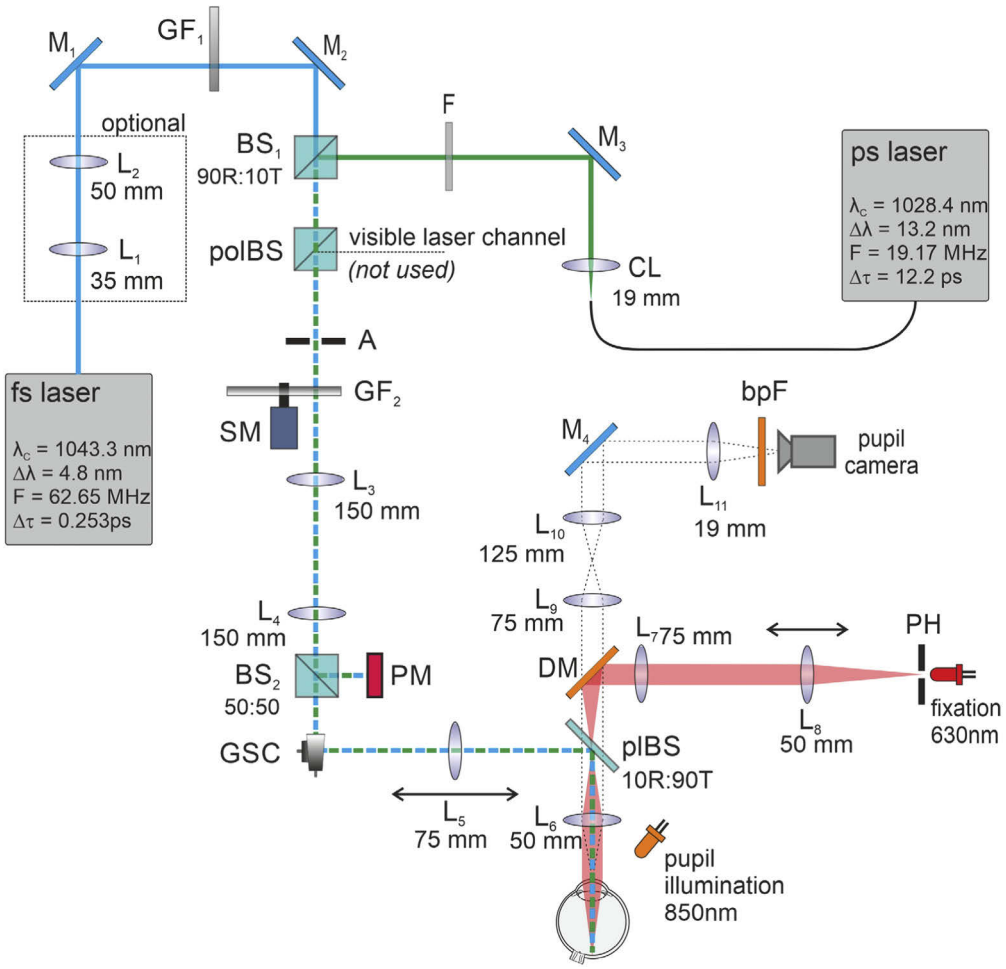

Fig. 1. Optical scheme of the measurement set-up. Symbols: L_i – lens, focal lengths are indicated, CL – collimating lens, M_i – mirror, GF_i – neutral density gradient filter, F – neutral density filter 1.0, BS_i – beamsplitter, polBS – polarization beamsplitter, A – aperture, SM – stepper motor, GSC – xy galvanometric scanners, PM – power meter sensor, plBS – plate beamsplitter, DM – dichroic mirror, PH – pinhole, bpF – bandpass filter.

varied from 0 to 4.0 controlled by a stepper motor, SM (ST4209X1004-A, Nanotec, 1/64 step operating mode). After the filter GF_2 and telescope L_3-L_4, approximately half the power of each stimulating beam was deflected to a power meter sensor PM (S120C, Thorlabs) by a beamsplitter, BS_2. The power meter indications were carefully calibrated before each round of measurements by using another sensor (S120C, Thorlabs) placed at the eye's pupil plane for each laser separately. Therefore, based on the indications of PM, the actual power of each laser at the pupil plane was determined. The galvanometric scanners GSC, optically conjugated (by L_5 and L_6) with the eye's pupil, were used to shape the stimulus and determine its retinal location. The movable lens L_5 permitted correction of the refraction of the subject's eye. The plate beamsplitter plBS (BSN11R, Thorlabs) was placed in the Fourier plane of the 4-*f* system consisting of L_5 and L_6. The plBS combined the optical path of the stimulating beams with the paths of the pupil camera and fixation. The maximal power of both lasers measured by the optical sensor at the eye's pupil

Biomedical Optics EXPRESS

plane did not exceed 400 μW, in accordance with safety limits. The $1/e^2$ widths of laser beams at the eye's pupil plane were equal to 1.5 mm and 2.1 mm for *fs laser* and *ps laser*, respectively.

Pupil size and its position were continuously monitored during the measurements using a monochrome camera (DCC1545M, Thorlabs) and infrared illuminator with central wavelength 850 nm (30 nm Full-Width at Half-Maximum (FWHM) bandwidth). Most of this radiation was transmitted by the beamsplitter plBS and the dichroic mirror DM (visible cold mirror FM03R, Thorlabs) placed after plBS, which coupled the optical path of the pupil camera with the fixation path. The image of the pupil was formed on the camera by two telescopes, consisting of lenses L_6-L_9 and L_{10}-L_{11}. The overall magnification of the pupil at the camera was equal to 0.23. The bandpass filter bpF (FB850-40, Thorlabs), placed in front of the camera, cut off the reflections of the stimulating beams. Images of the subject's pupil were continuously acquired during the measurements and stored for further analysis. The image was a square of 512×512 pixels. All pupil images were acquired with a frame rate of about 11 frames per second, and the exposure time was adjusted to about 40 ms per frame.

The fixation point, a faint red dot in the middle of the visual field used by the subjects to fix their gaze, was formed by an image of a 50-μm pinhole (PH in Fig. 1). Back-illuminated with a 630-nm diode, it was optically conjugated with the subject's retina using two telescopes formed by L_8 and L_7 as the first 4-*f* system and L_6 and the eye's lens as the second one. Movable lens L_8 was used to correct the refraction error of the subject's eye.

2.2. Characterization of laser sources

The *fs laser* was a femtosecond solid-state laser (HighQ-2, SpectraPhysics), while the *ps laser* was a novel compact Yb-doped fiber laser (Jive, Fluence). The optical spectra of both lasers measured at the perimeter output are depicted in Fig. 2(a). The *fs laser* has a sech^2 shaped spectrum with a 1043.3 nm central wavelength, 4.84 nm bandwidth at FWHM, and 9.8 nm bandwidth at 10% of maximum intensity. The *ps laser* has a much broader, more structured spectrum with a central wavelength of 1028.4 nm and 26.9 nm bandwidth at 10% of maximum intensity (in this case, the FWHM value provides no meaningful information as it cannot be directly translated to Fourier-limited pulse duration, and therefore it is not given). We also verified the shape of the spectrum directly at each laser output. No significant alterations were observed, confirming that no unexpected changes occurred in the optical setup (see section S1 and Fig. S1 in Supplement 1). Detailed parameters of both laser sources used in experiments are listed in Table 1.

Table 1. Parameters of laser sources used in experiments.

	Central wavelength [nm]	Spectral bandwidth at 10% of maximum intensity [nm]	Pulse duration [ps]	Repetition rate [MHz]
fs laser	1043.3	9.8	0.253	62.65
ps laser	1028.4	26.9	12.2	19.17

The intensity autocorrelation trace for *fs laser* measured in the plane of the eye pupil is presented in Fig. 2(b) together with the sech^2 fitting function. The pulse duration after deconvolution is equal to 253 fs. The autocorrelation function measured for longer delays is shown in the inset and indicates that there are no pre- or post-pulses, which could possibly originate from parasitic reflections or multi-pulsing of the laser. Additional measurements with a photodiode and a 400 MHz-bandwidth oscilloscope confirmed single-pulse operation in the nanosecond timescale. The FWHM of the optical spectrum and the pulse duration measured in the eye plane result in a time-bandwidth product (TBP) of 0.34. TBP for transform-limited pulses is 0.315, indicating that pulses are only slightly chirped. The intensity autocorrelation trace measured for *ps laser* is fitted with a Gaussian function (Fig. 2(c)), which is a typical pulse shape for mode-locked fiber

Biomedical Optics EXPRESS

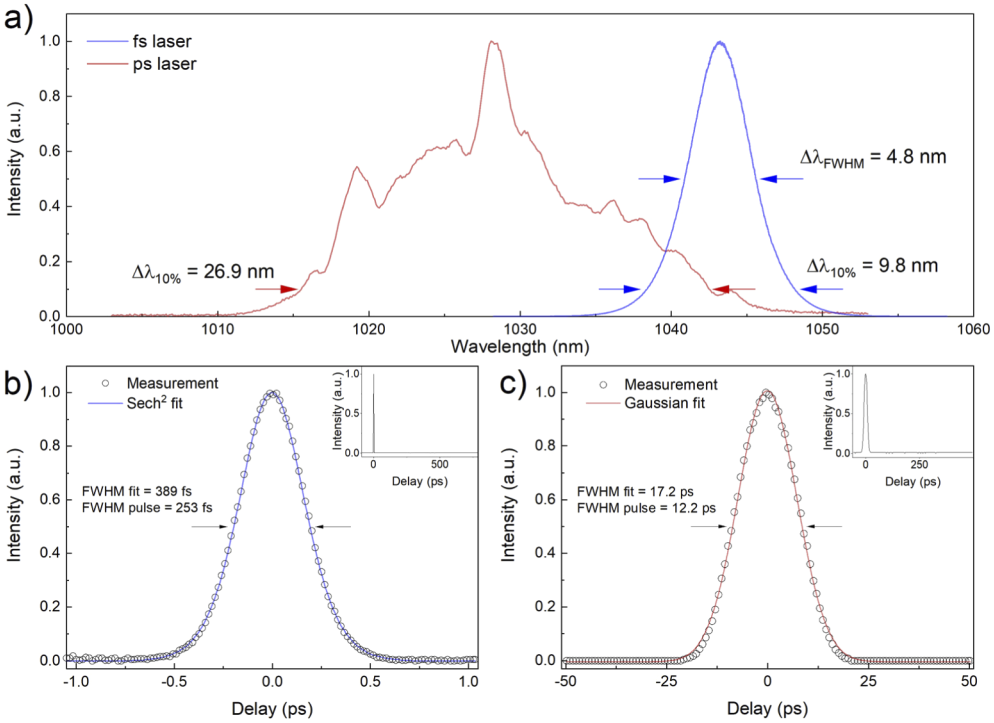

Fig. 2. Spectral and temporal properties of lasers used for producing visual stimulus. a) Optical spectra of *fs laser* and *ps laser* measured at the eye's pupil plane. b) Autocorrelation of *fs laser* pulse with sech^2 fitting function measured in the eye plane; inset shows the autocorrelation measured in a larger span of 900 ps. c) Autocorrelation of *ps laser* pulse with Gaussian fitting function measured in the eye plane; inset shows the autocorrelation measured in a larger span of 600 ps.

lasers operating in a normal dispersion (i.e. larger than zero) regime [24], in which the group velocity decreases with increasing optical frequency. The pulse duration in the eye plane is 12.2 ps. Similar to the previous case, a single pulse operation was confirmed by the autocorrelation measurement with longer delays (shown in the inset of the figure) and a pulse train visualization on the oscilloscope. The long pulse duration together with a broad optical spectrum indicates that the pulses are strongly chirped, which is typical for this kind of laser [24].

2.3. Psychophysical testing

During the experiments, a series of stimuli at different brightness was displayed on a subject's retina. Tested volunteers were asked to push the button when they registered the stimulus. A so-called 4-2-1 threshold-finding strategy, well-known from commercial perimeters [25,26], was implemented in the experiment control software written in LabVIEW. The algorithm, shown schematically in Fig. 3(a), is based on the stimulus intensity changes with decibel steps: 4 dB, 2 dB, and 1 dB. First, the stimulus power decreased with 4 dB steps until the subject was unable to see it (i.e. did not push the button within 2.5 s from the onset of the stimulus). Then, the power increased with one 2 dB step. In the next round, dependent on the previous subject's answer, the power was increased or decreased with 1 dB step. Assuming that lapses of volunteer causing false positive or false negative answers are rare, the 4-2-1 algorithm allows the threshold to be determined with the accuracy of 1 dB as illustrated in Fig. 3(a).

Biomedical Optics EXPRESS

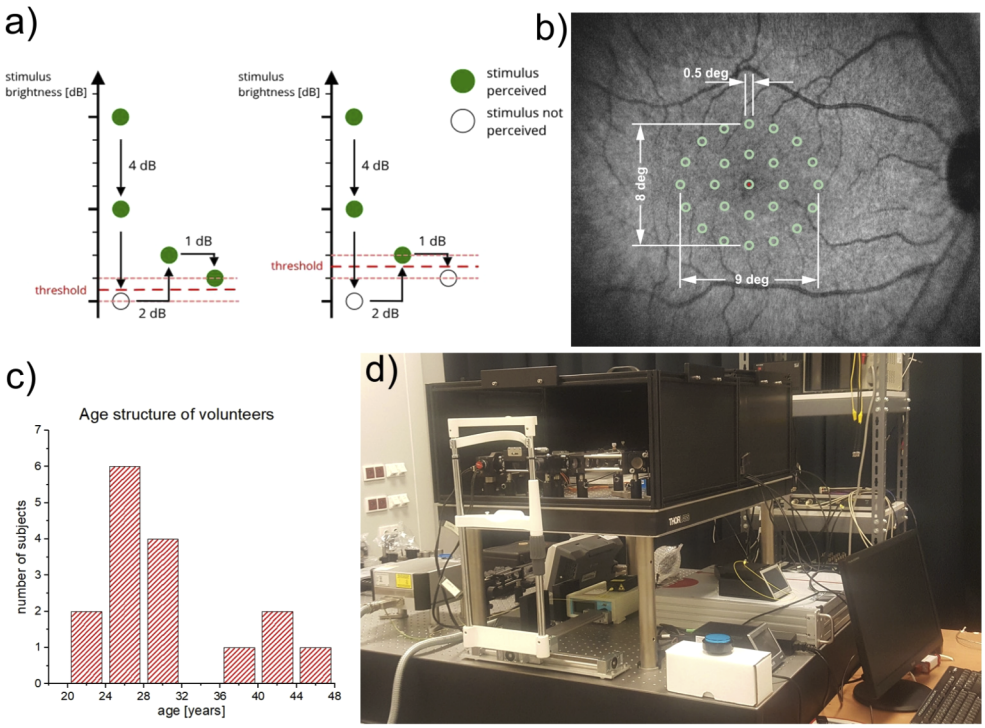

Fig. 3. The details of psychophysical tests. a) 4-2-1 threshold strategy: stimulus registered as seen: green circles, stimulus registered as not perceived: white circles; the range of intensities with a non-zero probability of registration of stimulus lies between short-dashed red lines, two boundary locations of this range are shown on left and right scheme. b) The grid of tested retinal locations (green circles), red dot indicates the position of fixation. c) Age distribution of the volunteers. d) Photo of the system.

Two-photon threshold T_{2P} was calculated as a geometric mean of lowest power of perceived stimulus P_{L} and highest power of not perceived stimulus P_{H}:

$$T_{2P} = \sqrt{P_L \cdot P_H} \tag{1}$$

To make the procedure shorter - for the convenience of the subjects - we also added a step to determine the initial intensity for all retinal points: at the beginning of a session the threshold was tested at the fovea center. The last value at which the subject was able to see the stimulus at this location was then used as the initial value for the rest of the locations from the grid. This value was always higher than visual thresholds at the rest of the locations, because for a healthy dark adapted subject, sensitivity, defined as an inverse of the visibility threshold, at the fovea center is lower than at other positions [27].

The visibility tests were performed using a circle stimulus of a diameter equal to 0.5 deg (Goldmann size III) scanned on the retina with a stimulating beam deflected by galvanometric scanners and a repetition rate of scanning was equal to 100 Hz. This shape was displayed intermittently for 0.2 s every 0.8 s (25% duty cycle). Sensitivity was tested in 25 retinal locations as shown in Fig. 3(b). The grid was slightly ellipsoidal: the outer ellipse's horizontal axis was equal to 9 deg, while the vertical axis was 8 deg. For every subject, the right eye was investigated. The red fixation point was located at the center of the fovea, inside the central stimulus.

Biomedical Optics EXPRESS

2.4. Measurement procedure and investigated subjects

We tested 16 volunteers (7 women and 9 men) 21 to 46 years old with normal vision and no history of ocular diseases. The exact age distribution of the tested subjects is shown in Fig. 3(c). All tests were performed after obtaining written informed consent, and all procedures complied with the Declaration of Helsinki and were approved by the Ethics Committee of the Collegium Medicum, Nicolaus Copernicus University in Torun.

All measurements were performed in a dark room (<0.01 lux) with dark adapted subjects and with use of apparatus shown in Fig. 3(d). Before the first psychophysical test, the adaptation period lasted for 30 minutes, with eye patches on both eyes. One measurement for a grid of 25 retinal locations lasted for 8 to 10 minutes. Between subsequent tests, a shorter period of 10 minutes for adaptation was applied. For 5 subjects (P6, P13, P14, P15, P17) the measurement procedure started with *fs laser*, for 9 other subjects the procedure started with *ps laser*, and for 2 subjects (P2, P16) the measurements were performed on different days. The subject's pupil was dilated with 1% Tropicamide drops applied before the first adaptation period. The protocol required that subjects remain for considerable periods in complete darkness, carefully looking for barely visible light stimuli and being ready to react at the appropriate time. We gathered 15 maps for *fs laser* (no map for P14) and 15 maps for *ps laser* (no map for P4).

During the measurements, the beam average power of either laser at the pupil plane was kept below 400 μW, which is below the ANSI Z136.1:2014 limits calculated for multiple pulse exposure lasting for 1 hour for stationary spot. According to Rule 2, which is the most restrictive for high repetition rate pulse trains (as in the case of both lasers being tested) and assuming an immobilized eye, 3600 s exposure for *fs laser* gives a maximum permissible exposure (MPE) equal to 4.07 J/cm^2 and maximum average radiant power (MPΦ) through a 7 mm pupil equal to 435 μW, while for *ps laser* MPE = 3.79 J/cm^2 and MPΦ = 405 μW [28].

2.5. Automated pupil recognition algorithm

The actual location of the stimulated region of the retina depends on the subject's fixation stability during the test. We used the images from the pupil camera to immediately correct the patient's eye position during measurements and for the analysis of the stability of the eye performed after the tests, in post-processing. For the latter case, the automated pupil recognition algorithm was necessary because we registered up to 20,000 pupil images during each test. The algorithms described in the literature [29–32] were not reliable for our images due to a variety of factors, like the size of the pupils on the image and heterogeneous light conditions caused by the pupil illuminator. Facing this issue, we developed a new approach for a fast and accurate pupil recognition algorithm. The algorithm is briefly described in Supplement 1(see Section S1, Fig. S2) and more details can be found in our previous work [33].

3. Results

3.1. Two-photon vision sensitivity of volunteers measured for both lasers

The result of testing is the acquisition of the *two-photon threshold* T_{2P} at 25 retinal locations, determined by the Eq. (1), expressed in Watts. The averaged maps for both lasers are presented in Fig. 4. Error bars indicate standard deviations (SD) of the mean for all tested subjects. For every investigated volunteer, the threshold power value was higher for *ps laser* than for *fs laser*. The mean threshold value (± one standard deviation) for the *fs laser* was 8.3 ± 6.3 μW for the central location; and 2.1 ± 1.1 μW for other locations (the error here is the mean of standard deviations for each location). For the *ps laser* the corresponding thresholds values were: 33.4 ± 21.3 μW and 8.0 ± 3.7 μW, respectively.

The two laser sources differ considerably in terms of pulse duration and repetition rate. While an optical sensor would indicate the same average power for short pulses of high frequency, long

Biomedical Optics EXPRESS

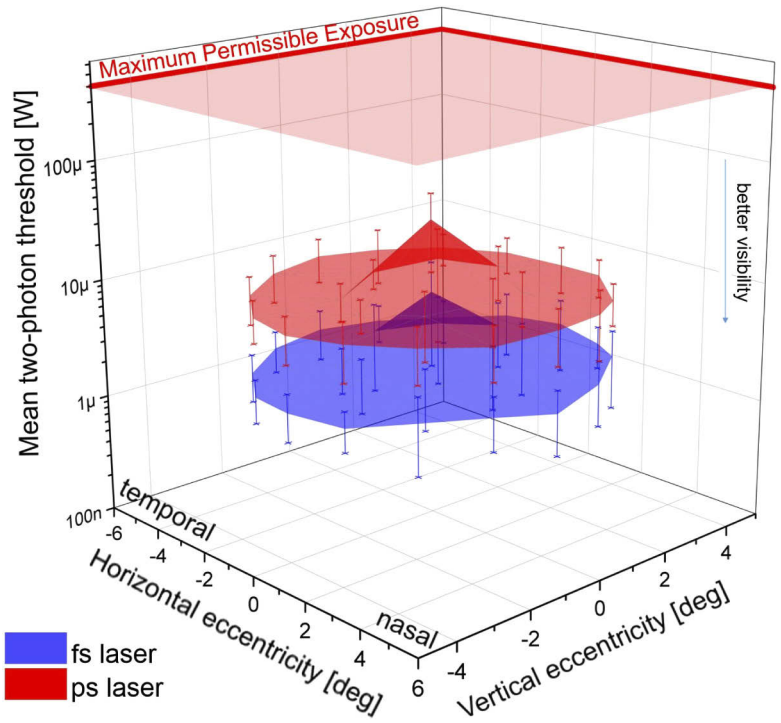

Fig. 4. Average maps of two-photon threshold (T_{2P}) for both lasers. The T_{2P} threshold value was averaged in each point for all subjects, the error bars are plotted for one standard deviation. The MPE level is indicated as the semi-transparent red plane at the top of the graph.

pulses of low frequency and, in the limit, a continuous wave source, the two-photon absorption rate would be completely different in these situations [34,35] and, consequently, their two-photon visibility as well. To assess if the observed differences in the two-photon vision threshold for both lasers are caused primarily by differences in pulse duration and repetition frequency, we performed some simple numerical modeling.

Laser pulse temporal power shapes $P_i(t)$, where i denotes either *fs laser* or *ps laser*, were approximated with normalized $\text{sech}^2(t)$ of 253 fs FWHM for *fs laser* and a Gaussian function of 12.2 ps FWHM for *ps laser*, according to autocorrelation measurement results and the manufacturer's specifications. Pulse repetition rates ($F_{rep,i}$) for both lasers were measured with a photodiode and equaled $F_{rep,\,fs} = 62.65$ MHz and $F_{rep,ps} = 19.17$ MHz. The number of two-photon events, i.e. isomerizations, $N_{2P,i}$ is proportional for each pulse train to an integral of squared instantaneous power, with factor C encompassing all process efficiency parameters, which are common for both lasers (such as quantum efficiency, two-photon absorption cross-section, beam geometry and visual pigment concentration) due to similar central wavelengths, beam sizes and the same subjects [12,35]:

$$N_{2P,i} \propto C \cdot \int_0^{t_{\text{exp}}} P_i^2(t)dt \tag{2}$$

To account for differences in repetition rates between pulses, the integral in Eq. (2) is calculated from $t = 0$ to $t = t_{exp}$, where t_{exp} is exposure time, which is much longer than single pulse duration. Subsequently, the *ps laser* power was adjusted in the model so $N_{2P,ps} = N_{2P,fs}$. In this situation

Biomedical Optics EXPRESS

of equal average numbers of two-photon induced isomerizations, the calculated relationship between two-photon thresholds for both lasers, $T_{2P,ps}/T_{2P,fs}$ is 3.6. The rationale behind the model is described in Supplement 1(section S2 and Fig. S3). According to this calculation, the average power of *ps laser* needs to be 3.6 times higher than the power of *fs laser* for obtaining the same visibility threshold for the human eye for both lasers. In our measurements the average threshold power of *ps laser* was 3.9 times higher than for *fs laser*. Our result is in good agreement with the expected threshold ratio by taking into account the spread of the obtained thresholds (SDs for both lasers are at the level of 50% of mean threshold value). However, other factors (spectral and geometric differences between both laser beams) might also influence this result, and are discussed in detail in Section 4.

Further, for compatibility with established methods of presenting the results in perimetry, we recalculated the T_{2P} values for *two-photon sensitivity* (S_{2P}) using the same equation as in [36]:

$$S_{2P}[dB] = 10 \log \frac{T_{MPE}}{T_{2P}} \tag{3}$$

where T_{MPE} was the same for both lasers and equal to 400 μW (MPE level and also the maximum average power permitted for each laser by the apparatus) and T_{2P}, the two-photon visibility threshold. The resulting average sensitivity map is shown in Fig. 5. Sensitivity maps for individual subjects are also shown in the Supplement (section S2, Figures S4 and S5).

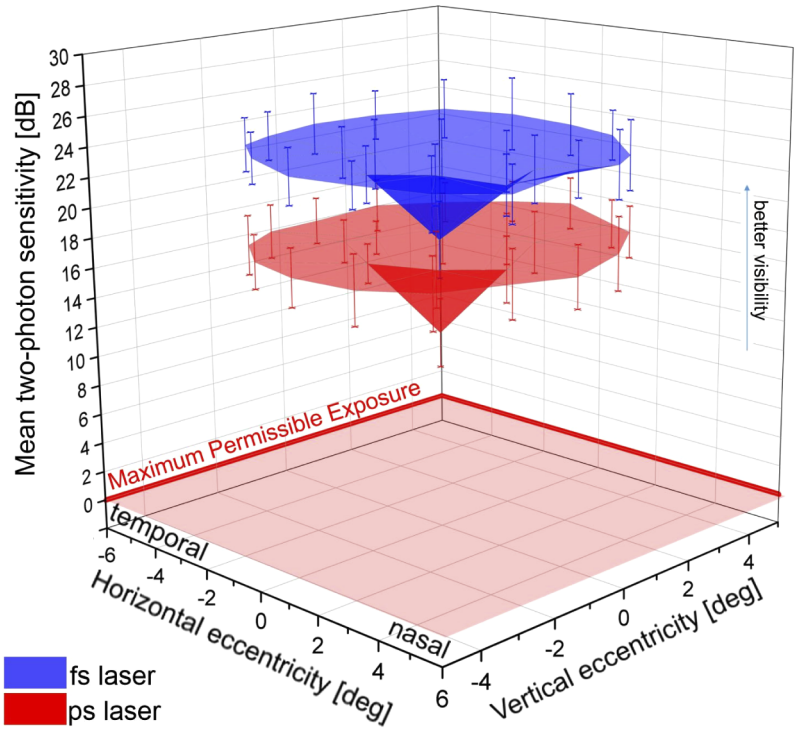

Fig. 5. Average maps of two-photon sensitivity (S_{2P}) for both lasers. The S_{2P} sensitivity value was averaged in each point for all subjects; the error bars are plotted for one standard deviation. The MPE level is indicated as the semi-transparent red plane at the bottom of the graph.

The mean sensitivity values for *fs laser* were: 17.7 ± 2.6 dB for central location and 23.4 ± 2.0 dB for the rest of the stimulated points. For the *ps laser* sensitivity values were equal to:

Biomedical Optics EXPRESS

11.4 ± 2.3 dB at fovea center and 17.4 ± 1.9 dB for the rest of locations. The thresholds ratio: $T_{2P,ps}/T_{2P,fs} = 3.6$ means that the expected sensitivity drop for *ps laser* in comparison to *fs laser* should be equal to 5.6 dB. It is less than the actual difference between means for whole maps which is 5.9 dB; however, it is within measurement uncertainty equal to 2.8 dB, calculated as a combined standard uncertainty.

The overall shape of the sensitivity maps for both lasers looks similar - the most pronounced difference is the shift of the whole map for *ps laser* towards lower sensitivities. To examine more closely the distribution of registered two-photon sensitivities in 25 tested retinal locations, the appropriate box charts are shown in Fig. S6. The locations were divided into three groups: central (Fig. S6a), inner ellipse of 4-4.5 deg size (Fig. S6b), and outer ellipse of size 8-9 deg (Fig. S6c). We performed one-way ANOVA tests between sensitivities obtained in different locations for each laser. Inside the group, there is no significant difference between tested sites for each laser; all points distributed on each ellipse are characterized by similar sensitivity. The box charts for each group of locations are shown in Fig. 6. As indicated with black stars, there is significant difference between both lasers for the particular group. There is no significant difference between the inner and outer ellipses for *ps laser*, but there is a statistically significant difference (p-value=0.024) between these ellipses for *fs laser*. It should be noted that for the center of the fovea (location 0) and the other two groups, there is a significant difference (p-value of the order of 10^{-16}). We also calculated ratios between medians for location 0 and the inner as well as outer ellipses for both lasers. For *fs laser* they were both marginally higher ($\approx$0.8) than for *ps laser* ($\approx$0.7). For all tested retinal locations, one-way ANOVA tests performed for the same location and different lasers indicated a significant difference (p-values of the order of 10^{-7} to 10^{-11}).

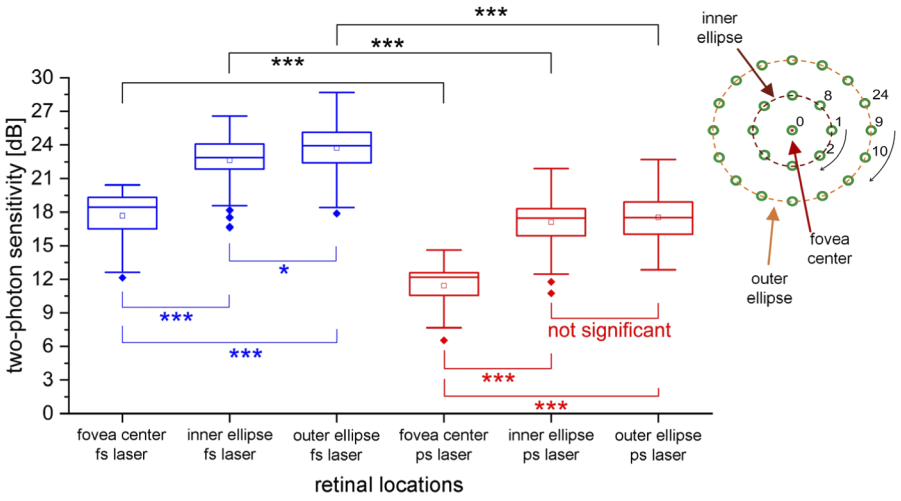

Fig. 6. Box charts plotted for two-photon sensitivity in three groups of tested locations: fovea center (location 0), inner ellipse (locations 1-8), outer ellipse (locations 9-24). Inset: numbering of locations. Labels: "not significant" – p-value > 0.05, * – p-value ≤ 0.05, *** – p-value ≤ 0.001.

The results, expressed as T_{2P} threshold maps as well as S_{2P} sensitivity maps, prove that the visibility of *ps laser* is lower than that of *fs laser*, and the relationship between locations of successive eccentricities are, in general, preserved for both lasers.

Biomedical Optics EXPRESS

3.2. Pupil position and pupil parameters

Position of the eye could change during test, which lasted about 10 minutes, affecting location of stimulating beam on the subject's retina. Moreover, even though the subject's pupil was dilated, a substantial shift from the center position in relation to the optical axis could cause beam vignetting. The pupil camera in the measurement system enables the operator to continuously monitor and correct the patient's eye position using an XYZ chinrest regulator. Eye images are presented in Fig. 7(a).

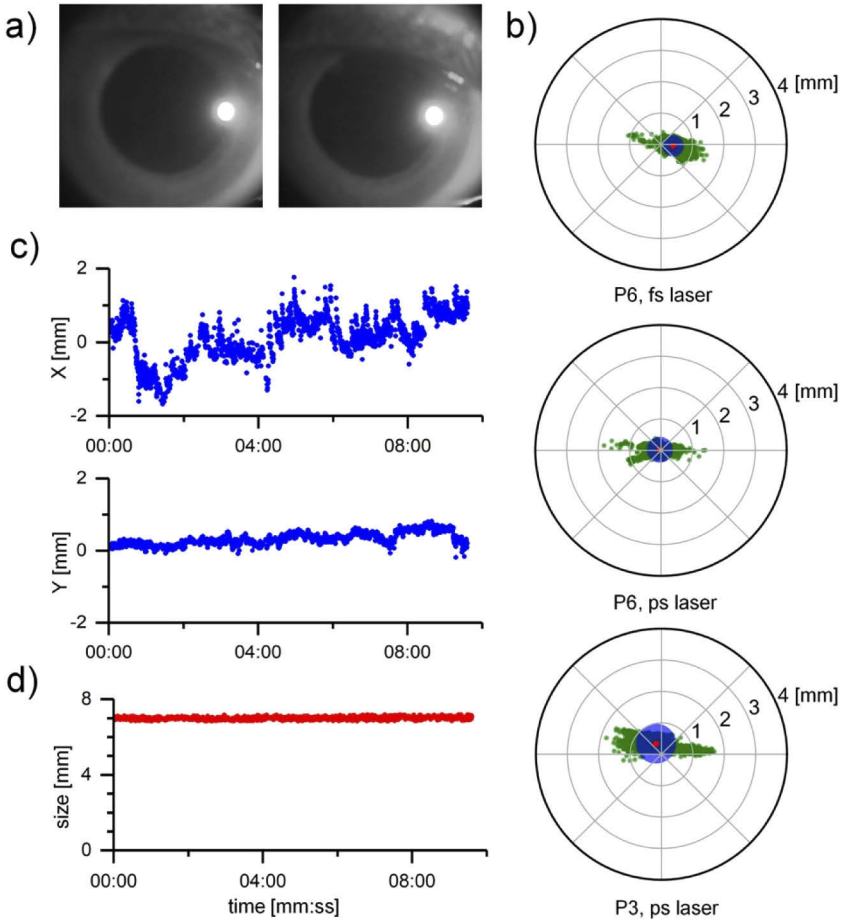

Fig. 7. Pupil parameters for selected patients. a) Example pupil camera images for the measurement for patient P3 and *ps laser*. b) Pupil center position for patient's right eye during the measurement. Center of the map corresponds to the center of the retina. Green dots - temporary pupil center positions; red dot and blue circle - mean pupil center position with one standard deviation, respectively. c) Changes of horizontal (X) and vertical (Y) position of pupil center during the measurement for patient P3 and *ps laser*. Position 0 corresponds to the center of the retina. d) Pupil diameter (size) as monitored during the measurement for patient P3 and *ps laser*.

Pupil camera images were further analyzed during post-processing. The procedure was divided into two parts: automated analysis by a dedicated program written in Python (described in Supplement 1, Section S1, Fig. S2) and filtration of the acquired raw data. During the analysis, numerical data describing the pupil (its center position and size) were obtained from gathered

Biomedical Optics EXPRESS

images. Filtration based on the numerical data permitted the omission of some photos for which the algorithm did not work properly, for example, when the images were recorded during blinking, or when the eye was partially-covered by the eyelid, or when the image was simply blurred. The results of post-processing were visualized as pupil position center maps, examples of which are shown in Fig. 7(b) and 7(c), and the pupil diameter size changes depicted in Fig. 7(d). All pupil data are shown in the Supplement (section S2, Fig. S7 and Fig. S8). Moreover, the mean eye position and its standard deviation were calculated. For all subjects, the average distance between the mean pupil center position and the center of the optical system was 0.26 ± 0.18 mm for *fs laser* and 0.26 ± 0.17 mm for *ps laser*. Also, for both lasers, the average standard deviation between the current pupil center position and the center of the optical system was below 0.5 mm. These numbers show that, for all measurements, the subject's eye position was correctly fixed during the test. Analysing the pupil size for all subjects, the mean pupil diameter was 7.49 ± 0.50 mm for *fs laser* and 7.76 ± 0.69 mm for *ps laser*. It confirms that the two-photon sensitivity values were unaffected by the lower power of the laser's beam due to vignetting.

Moreover, we also checked for any correlation between the patient's pupil parameters and the sensitivity data. For this purpose, we calculated the Pearson correlation coefficient (PCC) between the deviation from the mean value of the two-photon sensitivity values for both inner (Fig. 6(b)) and outer (Fig. 6(c)) ellipses and pupil parameters, such as the main pupil centre XY position, the main pupil centre position standard deviation, pupil diameter and its standard deviation, and the main distance between the pupil centre and optical centre of the system and its standard deviation. The calculations proved, that for any laser there is neither correlation between the deviation from the mean value of the two-photon sensitivity and pupil position nor its standard deviation (absolute value of PCC ≤ 0.5). This confirms that all subjects were positioned correctly during the experiments, and small deviations of the eye position during the test did not significantly influence the measured two-photon sensitivity values.

4. Discussion

Based on *two-photon vision*, we have developed a new method called *two-photon microperimetry* using short pulses of near-infrared light [14]. Two-photon microperimetry has already been successfully applied to medical ophthalmologic research to establish an average, normal level of scotopic two-photon sensitivity [36]. This study was conducted on 43 healthy subjects 20-70 years old. The results showed that the sensitivity does not significantly decrease with age, which is promising in the context of further practical implementation of this method [36]. The stimulation of the retina by an infrared beam that penetrates deeper and maintains its focal shape through opaque media also could be beneficial to visual field testing in patients with cataracts [14,37]. Two-photon absorption is confined to the focal region of the beam; therefore, the retina is stimulated only in this region. It results in remarkable contrast of two-photon perceived stimuli and can be used to further improve the accuracy of retinal stimulation, not only in advanced laboratory optical systems but also in simpler clinical instruments. In this paper we are testing compact fiber laser emitting pulses of duration in picosecond range as a light source in two-photon microperimetry.

It is difficult to quantify a purely physical phenomenon from psychophysical measurements. Even in a group of young, healthy volunteers, highly variable results are expected due to individual differences, including eye optics, visual processing, and nervous system function [38]. Therefore, the spread we measured for the absolute threshold values in the group of tested subjects is not surprising. The measured separation between the average two-photon sensitivities for both lasers is equal to 5.9 ± 2.8 dB, which agrees with the theoretical 5.6 dB sensitivity shift that corresponds to $T_{2P,ps}/T_{2P,fs}$ ratio for lasers pulse trains equal to 3.6. It should be mentioned that this shift to lower sensitivities still leaves a 17 dB range for testing two-photon vision of patients with visual

Biomedical Optics EXPRESS

defects, as shown in Fig. 5. Nevertheless, there are other differences between the tested lasers other than pulse duration and repetition frequency and that should be discussed as well.

The first factor that requires consideration is the spectral difference between *fs laser* and *ps laser*. The lasers strongly differ in spectral width, spectral shape as well as central maximum wavelength (Fig. 2(a) and Fig. 8), and these properties can impact the measured two-photon threshold.

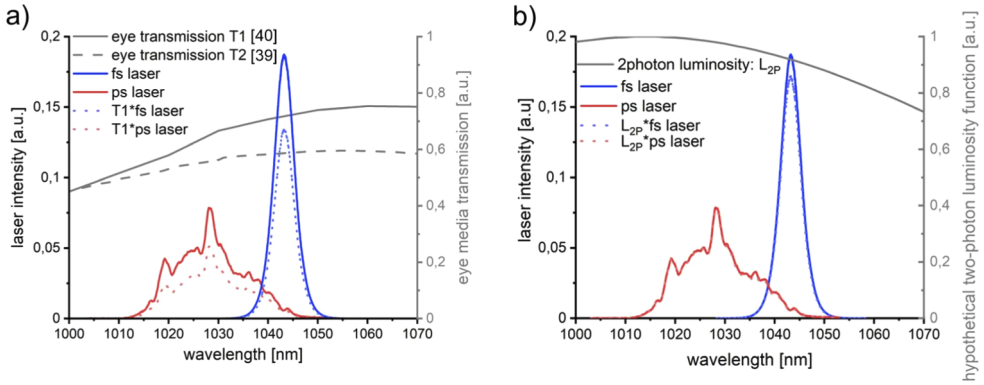

Fig. 8. Spectral properties of both laser sources. Spectra of *fs laser* and *ps laser* with normalized area: solid blue and red lines, respectively. a) Influence of ocular media transmission on laser visibility. Transmission data are based on [39]: grey dashed line and [40]: grey solid line. Spectra of *fs laser* and *ps laser* weighted by eye transmission curve T1: dotted blue and red lines, respectively. b) Influence of hypothetical two-photon scotopic luminosity function (solid grey line) on laser visibility. Spectra of *fs laser* and *ps laser* weighted by two-photon luminosity function: dotted blue and red lines, respectively; the change for *ps laser* is barely visible.

The stimulus light is transmitted through the ocular media to the retina, and the eye transmission increases with the wavelength in the spectral region of both lasers [39,40]. The main component responsible for the overall shape of eye transmission is water, thus the eye media can be approximated by a 22 mm layer of water [40]; the transmission curve is shown in Fig. 8(a) as a solid gray line. The transmission of all components of the ocular media (cornea, lens, aqueous humor, and vitreous) separately measured in human eyes post-mortem [39] and calculated as a product of them all, is shown as the dashed gray line. To assess how much the total photon flux of both lasers would be affected by eye media, we weighted their spectra with normalized area by eye transmission curve (solid gray line in Fig. 8(a)). The resulting modified spectra are shown in Fig. 8(a) as dotted blue and red lines for *fs laser* and *ps laser*, respectively. The ratio (A_2/A_1) of the calculated areas ($A_2 = 0.64$, $A_1 = 0.72$) under weighted spectra of *ps laser* and *fs laser*, respectively, measures the relative change in intensity and is equal to 0.89. It means that approximately 11% more photons of the *ps laser* beam would be absorbed in ocular media before reaching the retina plane resulting in a decrease of eye sensitivity for *ps laser* compared to *fs laser*.

Differences in the shape of the spectra could also affect the perceived brightness of both lasers. For one-photon vision, photometric quantities are used to compare the brightness of light sources of different spectral shapes. Spectral sensitivity of the human eye, different in photopic and scotopic conditions, can be described by efficiency curves to calculate the luminous intensity of sources of known spectral power distributions [41]. Obviously, the efficiency curves are established for one-photon vision, and the longest wavelength for which these curves were determined is 780 nm [42]. The shape of two-photon efficiency curves is still unknown and requires further investigation. However, based on our results [12,43], we propose, as a first

Biomedical Optics EXPRESS

approximation, to simply shift the one-photon scotopic sensitivity curve to the longer wavelength region by multiplying the wavelength by two. This approximation is shown as a solid gray line (L_{2P}) in Fig. 8(b). With this curve we can subsequently calculate the relative "*two-photon luminosity*" (scotopic) of our light sources. The spectra weighted with this hypothetical two-photon efficiency are shown with dotted blue and red lines. The ratio of areas under the weighted curves would be a measure of the relative difference in the brightness of both lasers for one-photon vision. The two-photon isomerization rate and consequently the perceived stimulus brightness are proportional to the square of the average power of the beam [14]. Therefore, a four times brighter source has only twice more power. Thus, we should also square the ratio of the calculated areas to get the appropriate relative difference in two-photon brightness between tested lasers. For the proposed *two-photon luminosity* curve L_{2P}, *ps laser* would be perceived as 1.13 times brighter $(0.98/0.92)^2$ than *fs laser*.

In summary, the effect of both spectral factors, eye media transmission (0.89) and two-photon spectral efficiency (1.13), on two-photon threshold appears to cancel each other ($0.89 \cdot 1.13 \approx 1.00$).

Focusing the beam in the retinal plane would also influence the two-photon absorption rate. In our experiment, beam diameters of both lasers in the pupil plane were equal to 1.5 mm for *fs laser* and 2.1 mm for *ps laser*. Assuming the diffraction limited focusing by an aberration-free eye, the beam of *fs laser* would produce a larger spot on the retina (15 µm diameter) than the beam of *ps laser* (10 µm diameter) assuming a monochromatic Gaussian beam and a 17 mm focal length of the eye. The *ps laser* has also a broader spectrum, which can cause more chromatic aberrations and thus greater deviations from the diffraction limited case than *fs laser*. To resolve questions about the possible effects of beam diameter on the measured visibility threshold, we carried out additional measurements with the beam of *fs laser* expanded to 2.2 mm at the pupil plane. For this purpose, we introduced a magnifying telescope (see Fig. 1) consisting of lenses L_1 and L_2 in the optical path of *fs laser*. We repeated the sensitivity measurements for *fs laser* for five participants and found that it did not influence the results (see section S3 of Supplement 1, Fig. S9). The mean value of the two-photon sensitivity for the expanded beam of the *fs laser* map is 23.4 ± 1.8 dB, compared to 23.4 ± 2.0 dB. This result proves that the differences between beam diameters in the pupil plane did not alter the result, however it is surprising and requires additional comments. First of all, the sensitivity of the 4-2-1 strategy is ±0.5 dB, which influences the ability to distinguish very small visibility differences. Secondly, there are two physical phenomena that need to be considered for a laser beam entering the eye: (1) a laser beam with a larger beam diameter will be focused into a smaller point at the retina than a beam with a smaller diameter, and (2) the aberrations in the eye affecting the entering laser beam quality are smaller for a beam with a smaller diameter than for a beam with a larger one, as shown, e.g., in Wilson et al. [44]. Probably these two effects compensate enough for differences to be not noticed during the experiments using the 4-2-1 threshold finding strategy. A third reason might be individual differences between subjects leading to blurring of the results as well. As it is known from the literature, the spot size focused on the retina has at least 30% systematic error (10 µm instead of 7 µm as the theoretical value for a 633 nm laser and 1.2 mm illuminating beam) reported by Birngruber et al. [45]. Theoretically, for beams with a diameter of 1.5 mm ($1/e^2$) and 2.1 mm we have 15 µm and 11 µm spot sizes on the retina, which are within the systematic error range introduced by the natural optics of the eye. Therefore, the results of the sensitivity thresholds do not differ significantly. For greater differences in beam sizes, separate experimental work should be carried out, which we plan in the future.

To explore the possibility of causing the two-photon vision sensation with other laser pulse temporal regimes in a similar microperimetry system (assuming the same experimental conditions, spectral range and beam geometry), we used our numerical model combined with the threshold power values found in our experiments. We wanted to find the pulse train patterns which would

Biomedical Optics EXPRESS

be expected to excite a similar number of two-photon isomerizations (be visible to potential subjects) but still have less average power than the MPE level, so in principle be safe to use in an experiment. As the region of interest we selected nanosecond pulses which have been reported to cause two-photon visibility in OCT systems in the past [21,22]. It is worth noting that in that case the two-photon visibility is an unwanted phenomenon, so our calculation could help in the design of imaging devices employing nanosecond sources to avoid the illumination light being visible to patients. We set the average power in our calculation to 400 μW (just below MPE in our conditions) and modelled nanosecond regime pulses with the integral of their power squared equal to that of the pulses which we used in the experiment (i.e. causing the same nonlinear effect on the retina). Two-photon visibility can be obtained with a continuum of pulse train characteristics; but as an example we numerically found the pulse train combining 470 ns sech^2(t) pulses at a 1 MHz repetition rate (1000 ns intervals) to be a good two-photon vision-exciting candidate. It should be noted that this pulse train exhibits nearly 50% duty cycle, so serious questions of applicability of pulsed laser-related safety norms arise. Possibly the MPE level should be evaluated more carefully here, taking into account not only existing tabulated norms but also specific physical phenomena in the tissue, analogous to the detailed safety discussion in [12].

5. Conclusions

In this report we show how the retinal sensitivity of subjects with normal vision decreases after changing from a solid-state laser emitting sub-picosecond pulses to a fiber laser emitting picosecond pulses. The observed decrease of two-photon sensitivity (5.9 ± 2.8 dB) can be explained by accounting for the pulse duration and repetition frequencies of both lasers. This relatively small decrease of sensitivity means that fiber lasers with picosecond pulses can be successfully used for studying two-photon vision, and ultimately incorporated into clinical instruments.

Funding

Narodowe Centrum Nauki (2016/23/B/ST2/00752); City of Gdynia (3/DOT/2016); Fundacja na rzecz Nauki Polskiej (MAB/2019/12, POIR.04.04.00-00- 3D47/16-00); Horizon 2020 Framework Programme (666295); Ministerstwo Nauki i Szkolnictwa Wyższego (2016-2019).

Acknowledgments

K.K. wishes to acknowledge the National Science Centre and the City of Gdynia. K.P. is the Irving H. Leopold Chair of Ophthalmology. The authors also acknowledge support from an RPB unrestricted grant to the Department of Ophthalmology, University of California, Irvine. The International Centre for Translational Eye Research (MAB/2019/12) project is carried out within the International Research Agendas programme of the Foundation for Polish Science co-financed by the European Union under the European Regional Development Fund.

Disclosures

GP: Polgenix (E,P). KP: Polgenix (C), University of Washington (P). MW: Polgenix (P). KK: Polgenix (P).

See Supplement 1 for supporting content.

Biomedical Optics EXPRESS

References

1. C. A. Johnson, "Visual Fields: Visual Field Test Strategies," in *Pearls of Glaucoma Management*, J. A. Giaconi, S. K. Law, A. L. Coleman, K. Nouri-Mahdavi, and J. Caprioli, eds., 2nd ed. (Springer-Verlag, 2016), pp. 123–128.
2. K. Rohrschneider, S. Bültmann, and C. Springer, "Use of fundus perimetry (microperimetry) to quantify macular sensitivity," Prog. Retin. Eye Res. **27**(5), 536–548 (2008).
3. E. Midena, S. Vujosevic, E. Convento, A. Manfre', F. Cavarzeran, and E. Pitotto, "Microperimetry and fundus autofluorescence in patients with early age-related macular degeneration," Br. J. Ophthalmol. **91**(11), 1499–1503 (2007).
4. A. Molina-Martín, R. J. Pérez-Cambrodí, and D. P. Piñero, "Current clinical application of microperimetry: a review," Semin. Ophthalmol. **33**(5), 620–628 (2018).
5. R. J. Jamara, F. Van De Velde, and E. Peli, "Scanning eye movements in homonymous hemianopia documented by scanning laser ophthalmoscope retinal perimetry," Optom. Vis. Sci. **80**(7), 495–504 (2003).
6. R. W. Beck, T. J. Bergstrom, and P. R. Lighter, "A clinical comparison of visual field testing with a new automated perimeter, the humphrey field analyzer, and the goldmann perimeter," Ophthalmology **92**(1), 77–82 (1985).
7. M. Crossland, M.-L. Jackson, and W. H. Seiple, "Microperimetry: a review of fundus related perimetry," Optom. Rep. **2**(1), 2 (2012).
8. B. Bengtsson, J. Olsson, A. Heijl, and H. Rootzén, "A new generation of algorithms for computerized threshold perimetry, SITA," Acta Ophthalmol. Scand. **75**(4), 368–375 (2009).
9. S. N. Markowitz and S. V. Reyes, "Microperimetry and clinical practice: an evidence-based review," Can. J. Ophthalmol. Can. d'Ophtalmologie **48**(5), 350–357 (2013).
10. W. S. Tuten, P. Tiruveedhula, and A. Roorda, "Adaptive optics scanning laser ophthalmoscope-based microperimetry," Optom. Vis. Sci. **89**(5), 563–574 (2012).
11. W. M. Harmening, W. S. Tuten, A. Roorda, and L. C. Sincich, "Mapping the perceptual grain of the human retina," J. Neurosci. **34**(16), 5667–5677 (2014).
12. G. Palczewska, F. Vinberg, P. Stremplewski, M. P. Bircher, D. Salom, K. Komar, J. Zhang, M. Cascella, M. Wojtkowski, V. J. Kefalov, and K. Palczewski, "Human infrared Vision is triggered by two-photon chromophore isomerization," Proc. Natl. Acad. Sci. U. S. A. **111**(50), E5445–E5454 (2014).
13. P. Artal, S. Manzanera, K. Komar, A. Gambín-Regadera, and M. Wojtkowski, "Visual acuity in two-photon infrared vision," Optica **4**(12), 1488–1491 (2017).
14. D. Ruminski, G. Palczewska, M. Nowakowski, V. Kefalov, K. Komar, K. Palczewski, and M. Wojtkowski, "Two-photon microperimetry: sensitivity of human photoreceptors to infrared light," Biomed. Opt. Express **10**(9), 4551–4567 (2019).
15. A. Zielińska, K. Kiluk, M. Wojtkowski, and K. Komar, "System for psychophysical measurements of two-photon vision," Photon.Lett.PL **11**(1), 1–3 (2019).
16. F. Vinberg, G. Palczewska, J. Zhang, K. Komar, M. Wojtkowski, V. J. Kefalov, and K. Palczewski, "Sensitivity of mammalian cone photoreceptors to infrared light," Neuroscience **416**, 100–108 (2019).
17. D. R. Griffin, R. Hubbard, and G. Wald, "The sensitivity of the human eye to infra-red radiation," J. Opt. Soc. Am. **37**(7), 546–554 (1947).
18. T. D. Lamb, "Photoreceptor spectral sensitivities: Common shape in the long-wavelength region," Vision Res. **35**(22), 3083–3091 (1995).
19. S. Gholami, L. Pedraza-González, X. Yang, A. A. Granovsky, I. N. Ioffe, and M. Olivucci, "Multistate multiconfiguration quantum chemical computation of the two-photon absorption spectra of bovine rhodopsin," J. Phys. Chem. Lett. **10**(20), 6293–6300 (2019).
20. S. Manzanera, D. Sola, N. Khalifa, and P. Artal, "Vision with pulsed infrared light is mediated by nonlinear optical processes," Biomed. Opt. Express **11**(10), 5603–5617 (2020).
21. T. Butler, S. Slepneva, B. O'Shaughnessy, B. Kelleher, D. Goulding, S. P. Hegarty, H. C. Lyu, K. Karnowski, M. Wojtkowski, and G. Huyet, "Single shot, time-resolved measurement of the coherence properties of OCT swept source lasers," Opt. Lett. **40**(10), 2277–2280 (2015).
22. S. Slepneva, B. O'Shaughnessy, B. Kelleher, S. P. Hegarty, A. Vladimirov, H.-C. Lyu, K. Karnowski, M. Wojtkowski, and G. Huyet, "Dynamics of a short cavity swept source OCT laser," Opt. Express **22**(15), 18177 (2014).
23. S. Manzanera, D. Sola, K. Komar, M. Wojtkowski, and P. Artal, "Two photon vision with a supercontinuum source," Invest. Ophthalmol. Vis. Sci. **60**(9), 5945 (2019).
24. J. Szczepanek, T. M. Kardaś, M. Michalska, C. Radzewicz, and Y. Stepanenko, "Simple all-PM-fiber laser mode-locked with a nonlinear loop mirror," Opt. Lett. **40**(15), 3500–3503 (2015).
25. "Microperimeter (MP-3) - NIDEK," https://usa.nidek.com/microperimeter-mp-3/.
26. "Maia - The New Frontier of Microperimetry," https://www.centervue.com/products/maia/.
27. A. J. Riopelle and W. J. Bevan, "The Distribution of Scotopic Sensitivity in Human Vision," Am. J. Psychol. **66**(1), 73–80 (1953).
28. F. C. Delori, R. H. Webb, and D. H. Sliney, "Maximum permissible exposures for ocular safety (ANSI 2000), with emphasis on ophthalmic devices," J. Opt. Soc. Am. A **24**(5), 1250–1265 (2007).
29. L. Świrski, A. Bulling, and N. Dodgson, "Robust real-time pupil tracking in highly off-axis images," in *ETRA '12: Proceedings of the Symposium on Eye Tracking Research and Applications* (2012), pp. 173–176.

Biomedical Optics EXPRESS

30. W. Fuhl, T. C. Santini, T. Kübler, and E. Kasneci, "ElSe: Ellipse selection for robust pupil detection in real-world environments," Eye Track. Res. Appl. Symp. **14**, 123–130 (2016).
31. W. Fuhl, T. Kübler, K. Sippel, W. Rosenstiel, and E. Kasneci, "ExCuSe: robust pupil detection in real-world scenarios BT - computer analysis of images and patterns," in *Computer Analysis of Images and Patterns. CAIP 2015. Computer Analysis of Images and Patterns. CAIP 2015. Lecture Notes in Computer Science*, G. Azzopardi and N. Petkov, eds. (2015), 9256, pp. 39–51.
32. T. Santini, W. Fuhl, and E. Kasneci, "PuRe: Robust pupil detection for real-time pervasive eye tracking," Comput. Vis. Image Underst. **170**, 40–50 (2018).
33. M. Martynow, A. Zielińska, M. Marzejon, M. Wojtkowski, and K. Komar, "Pupil detection supported by Haar feature based cascade classifier for two-photon vision examinations," in *2019 11th International Symposium on Image and Signal Processing and Analysis (ISPA)* (2019), pp. 54–59.
34. W. Denk, J. Strickler, and W. Webb, "Two-photon laser scanning fluorescence microscopy," Science **248**(4951), 73–76 (1990).
35. C. Xu and W. W. Webb, "Measurement of two-photon excitation cross sections of molecular fluorophores with data from 690 to 1050 nm," J. Opt. Soc. Am. B **13**(3), 481–491 (1996).
36. G. Łabuz, A. Rayamajhi, J. Usinger, K. Komar, P. Merz, R. Khoramnia, G. Palczewska, K. Palczewski, and G. U. Auffarth, "Clinical application of infrared-light microperimetry in the assessment of scotopic-eye sensitivity," Transl. Vis. Sci. Technol. **9**(8), 7–9 (2020).
37. A. Wei, U. V Mehta, G. Palczewska, A. M. Palma, V. M. Hussey, L. E. Hoffmann, A. Diep, K. Nguyen, B. Le, S. Y.-S. Chang, and A. W. Browne, "Two-Photon Microperimetry: A media opacity-independent retinal function assay," bioRxiv 2020.06.27.175315 (2020).
38. B. R. Hammond and J. Buch, "Individual differences in visual function," Exp. Eye Res. **199**(August), 108186 (2020).
39. E. A. Boettner and J. R. Wolter, "Transmission of the Ocular Media," Invest. Ophthalmol. Vis. Sci. 1(6), 776–783 (1962).
40. T. J. T. P. Van Den Berg and H. Spekreijse, "Near infrared light absorption in the human eye media," Vision Res. **37**(2), 249–253 (1997).
41. Y. Ohno, "Photometric standards," in *Handbook of Applied Photometry*, C. DeCusatis, ed. (American Institute of Physics, 1997), p. 59.
42. G. Wyszecki and W. S. Stiles, *Color Science: Concepts and Methods, Quantitative Data and Formulae* (John Wiley and Sons, 1983).
43. K. Komar, A. Zielinska, D. Ruminski, M. Marzejon, P. Ciacka, L. Kornaszewski, S. Manzanera, P. Artal, and M. Wojtkowski, "The limits of perception of light by two-photon vision," Invest. Ophthalmol. Vis. Sci. **60**(9), 3907 (2019).
44. B. J. Wilson, K. E. Decker, and A. Roorda, "Monochromatic aberrations provide an odd-error cue to focus direction," J. Opt. Soc. Am. A **19**(5), 833 (2002).
45. R. Birngruber, E. Drechsel, F. Hillenkamp, and V. P. Gabel, "Minimal spot size on the retina formed by the optical system of the eye," Int. Ophthalmol. **1**(3), 175–178 (1979).